*Article*

# Electrospun Core-Shell Nanofiber as Separator for Lithium-Ion Batteries with High Performance and Improved Safety

**Yun Zhao [1,*], Yanxi Li [2,*] and Zheng Liang [2,*]**

[1] Institute of Nuclear & New Energy Technology, Tsinghua University, Beijing 100084, China; yzhaozjut@tsinghua.edu.cn
[2] Department of Materials Science and Engineering, Stanford University, Stanford, CA 94305, USA; lianzhen@stanford.edu
* Correspondence: lianzhen@stanford.edu (Z.L.); yzhaozjut@tsinghua.edu.cn (Y.Z.); liyanxi@stanford.edu (Y.L.)

**Abstract:** Though the energy density of lithium-ion batteries continues to increase, safety issues related with the internal short-circuit and the resulting combustion of highly flammable electrolyte impede the further development of lithium-ion batteries. It has been well-accepted that a thermal stable separator is important to postpone the entire battery short-circuit and thermal-runaway. Traditional methods to improve the thermal stability of separators includes surface modification and/or developing alternate material systems for separators which may always affect the battery performance negatively. Herein, a thermostable and shrink-free separator with little compromise in battery performance is prepared by coaxial electrospinning and tested. The separator consists of core-shell fiber networks where poly(vinylidene fluoride-hexafluoropropylene) (PVDF-HFP) layer serves as shell and polyacrylonitrile (PAN) as the core. This core-shell fiber network exhibits little or even no shrinking/melting at elevated temperature over 250 °C. Meanwhile, it shows excellent electrolyte wettability and can take large amount of liquid electrolyte three times more than that of conventional Celgard 2400 separator. In addition, the half-cell using $LiNi_{1/3}Co_{1/3}Mn_{1/3}O_2$ as cathode and the aforementioned electrospun core-shell fiber network as separator demonstrates superior electrochemical behavior, stably cycling for 200 cycles at 1 C with a reversible capacity of 130 mAh $g^{-1}$ and little capacity decay.

**Keywords:** lithium-ion battery; safety; separator; coaxial electrospinning; dual-nozzle; core-shell nanofiber

---

## 1. Introduction

With the recent development of portable electronics and electric vehicles, there is a strong demand for advanced lithium-ion batteries (LIB) with high energy density [1-9]. Although the energy density of LIBs keeps increasing under the intensive research efforts, safety issues associated with internal short-circuit and the resulting combustion of flammable electrolyte impedes the further development and commercial application of next-generation LIBs [10]. It is well-accepted that the shrinking of separator under elevated temperature accelerates the battery shorting and thermal runaway process [11-14]. Therefore, advanced separators with improved thermal stability is of great significance for battery safety [15-19]. However, most modifications made to the separator could affect the battery performance negatively [20,21]. As a result, it is necessary to develop a novel battery separator with superior thermal stability and little compromise on battery performance.

Commercial separator (a combination of porous polyethylene (PE) film and porous polypropylene (PP) film) though being widely used for decades, suffers from poor thermal stability and limited electrolyte wettability [22,23]. Ceramic particle coatings are thereby developed and applied to these commercial separators to tackle the above problems [24-26]. Although the ceramic particles coated commercial separators exhibit improved electrolyte uptake and thermal stability [27,28], the LIBs using these coated separators show a reduced electrochemical performance due to the reduced separator pore size, increase in film thickness/weight, and poor adhesion between coating layer and separator layer [29-32]. Moreover, intensive research efforts have been placed to develop novel battery separators based on alternate material systems other than PE or PP, including polyacrylonitrile (PAN) [33], polyimide (PI) [34], poly(vinylidene fluoride-hexafluoropropylene) (PVDF-HFP) [35], and ether-modified poly(ether ether ketone) (PEEK) [36]. However the improvement is quite limited, and it is still challenging to achieve good mechanical strength, superior thermal stability, large electrolyte uptake, and little negative influence on electrochemical performance in the same time for a battery separator system [33-38].

Herein, following this line, we successfully design a core-shell fiber network by coaxial electrospinning to achieve both excellent thermal stability and electrochemical properties in the same time: the thermally-stable and mechanically-strong PAN fibers as the core serve as rigid framework to preserve the separator structure at elevated temperature; the PVDF-HFP as the shell layer covering on the PAN core provides excellent electrolyte wettability. To prepare this core-shell fiber network, coaxial electrospinning technique is employed (Figure 1). Typically, two syringes are connected into a dual-nozzle, and precursor solutions of PAN and PVDF-HFP are injected into the inner and outer channels of the dual-nozzle, respectively. Afterwards, the core-shell fiber network can thus be produced through this technique and can be used as dual-functional separators for LIBs with high performance and improved safety.

## 2. Materials and Methods

### 2.1 Materials

PAN (average $M_w$ = 150,000, powder), PVDF-HFP (average $M_w$ = 455,000; average $M_n$ = 110,000, pellets), dimethylformamide (DMF, 99.8%) and N-methyl-2-pyrrolidone (NMP, 99.5%) were purchased from Sigma-Aldrich. All of these reagents were used without further purification. Electrolyte (1 M $LiPF_6$ dissolved in a mixture of ethylene carbonate (EC) and diethyl carbonate (DEC) (v/v = 1:1), moisture < 10 ppm), commercial separator (Celgard 2400), poly(vinylidene fluoride) (PVDF, HSV900, 99.5%), carbon black C45, $LiNi_{1/3}Co_{1/3}Mn_{1/3}O_2$ (NCM), lithium metal foil (99.9%), copper foil (12 μm, 99.8%), aluminum (Al) foil (16 ± 2 μm, 99.54%) and coin cell type-CR2032 were purchased from MTI Kejing Technology.

### 2.2 Method

The core-shell fiber network which was used as battery separators was fabricated by dual-nozzle coaxial electrospinning. The core and shell precursor solutions were prepared by 8 wt% PAN and 12 wt% PVDF-HFP dissolved in dimethylformamide (DMF), respectively. In more details, the PAN precursor solution was prepared by dissolving 8 g PAN powder in 92 g DMF solution under stirring for 3 hr at 70 °C. The PVDF-HFP precursor solution was prepared by dissolving 12 g PVDF-HFP in 88 g DMF solution under stirring for 3 hr at room temperature. When both solutions became homogeneous, the solutions were treated in ultrasonic bath for 30 min to remove bubbles. The concentrations of our precursor solutions were set at a relatively low level because dilute solutions help a partially mixing of PAN and PVDF-HFP which leads to strong interaction during the electrospinning process. During electrospinning, 0.54 mL $h^{-1}$ of PAN precursor solution was extruded through the inner channel of the dual-nozzle while 1.08 mL $h^{-1}$ of PVDF-HFP precursor solution was extruded through the outer channel. Before voltage setup, it was important to extrude PVDF-HFP solution firstly than extruding PAN solution. The electrospinning voltage was set to 16 kV in the beginning and then gradually lowered to 14.8 kV to form a stable Taylor cone. This operation could avoid the deposition of solution droplets on the metallic collector. The obtained electrospun fiber network was dried at 60 °C and the thickness of this fiber network was controlled to be around 40 μm.

### 2.3 Characterization

The thermal gravimetric analysis (TGA, Netzsch, STA 409 PC) was performed in air at the heating rate of 10 °C $min^{-1}$. The morphology and elemental composition of the fiber network were examined by transmission electron microscopy (TEM, Hitachi, HT7700), scanning electron microscopy (SEM, Hitachi, SU-8010) and energy dispersive spectrometer (EDS, Hitachi, SU-8010).

To confirm the thermal behavior of the as-prepared separator, PAN@PVDF-HFP core-shell fiber network and PVDF-HFP fiber network were heated in a temperature range from 25 to 250 °C. The electrolyte uptake was measured by soaking the fiber network in 1 M $LiPF_6$ in EC/DEC electrolyte for 10 min, removing the residual electrolyte on the separator surface with air-laid paper and weighing the soaked separator three times to obtain an accurate measurement. The mass gain (average value) was therefore considered as the amount of electrolyte uptake. The contact angles of electrolyte droplets on different separators were studied using contact angle meter (Dataphysics, OCA15Pro).

### 2.4 Electrochemical Characterization

The $LiNi_{1/3}Co_{1/3}Mn_{1/3}O_2$ (NCM) half-cell was constructed using Li foil as the anode and NCM as the cathode to examine the influence of separators on battery performances. The results were compared between commercial separator and electrospun fiber networks. The NCM cathode was fabricated by mixing NCM powder, carbon black C45 and PVDF (8 wt% PVDF in NMP) with the weight ratio of 8:1:1. The resulting slurry was coated onto Al foil via a doctor-blade and the loading of active materials was controlled at about 3 mg $cm^{-2}$. The electrode was then dried in a vacuum oven in air at 120 °C for 24 hours. The CR2032 coin cell was assembled by sandwiching the as-prepared electrospun fiber network adding 80 μL electrolyte (1 M $LiPF_6$ in mixture of EC/DEC with ratio of 1:1 by volume) between a piece of NCM cathode disc and a piece of lithium foil disc. Galvanostatic discharge-charge cycling was performed with land system (CT2001A) in a potential range from 2.5 V to 4.2 V at 0.1 C in the first 3 cycles for activation and at 1 C in the following cycles.

## 3. Results and Discussion

The morphology of the as-prepared electrospun core-shell nanofiber (denoted as PAN@PVDF-HFP) is shown in Figure S1-S2. The diameter of each single fiber ranges from 300 nm to 500 nm without showing obvious agglomeration (Figure S1). From the TEM image, the core-shell structure is observed and confirmed (Figure S2). The as-prepared electrospun fiber network PAN@PVDF-HFP shows excellent flexibility, as no obvious cracks or defects can be observed after rolled up or scrunched several times (Figure S3), indicating that the outer PVDF-HFP layer provides sufficient mechanical support and protection to lead to an improved mechanical property.

Peer-reviewed version available at Energies 2019, 12, 3391; doi:10.3390/en12173391



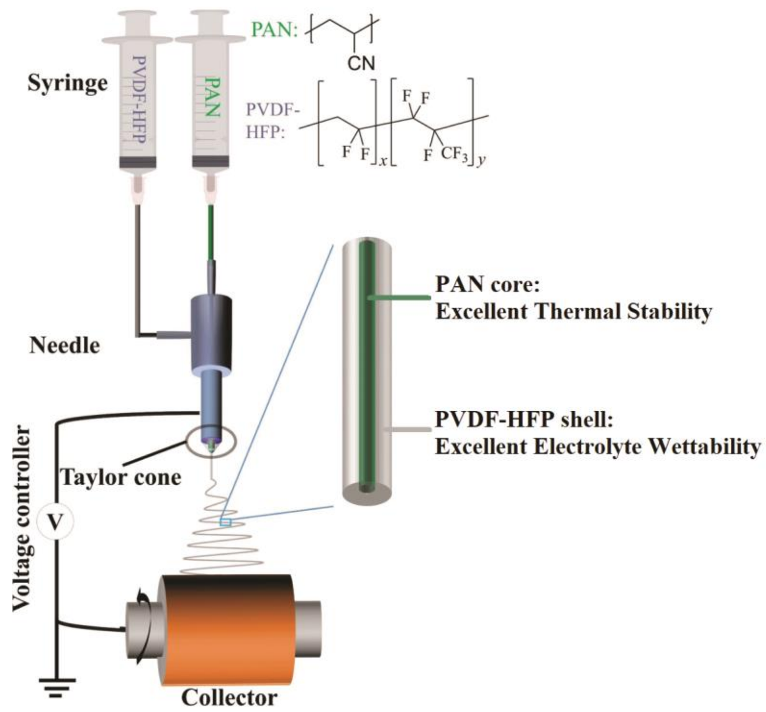


**Figure 1.** Schematic illustration of the fabrication process of PAN@PVDF-HFP fiber using dual-nozzle coaxial electrospinning technique. The PAN and PVDF-HFP precursor solutions are injected by syringes into the core and shell channels of the needle, respectively. The PAN core with excellent thermal stability serves as framework to preserve the entire structure at elevated temperature.

The content of PAN in the PAN@PVDF-HFP separator is determined by TGA (Figure 2a). Pure PAN powder exhibits a three-step decomposition: the first characteristic weight loss peak is sharp and clear with about 30% loss occurring at around 300 °C; the second weight loss behavior occurs in the temperature range of 300 °C to 470 °C followed by the third weight loss which is around 500-600 °C. The weight loss of PVDF-HFP can be divided into two steps at around 450 °C and in the region of 450 °C to 520 °C. For PAN@PVDF-HFP core-shell nanofiber, the first weight loss at 300 °C is very similar to the first characteristic sharp weight loss peak of PAN counting for about 30% loss and the rest region on the curve behaves like a mixture of PAN and PVDF-HFP. Therefore this sharp peak at 300 °C is used to calculate the content of PAN in the polymer mixture. Specifically, this peak at 300 °C related to 30 wt% weight loss for pure PAN corresponds to an estimation of about 15%-17% total loss in the PAN@PVDF-HFP composite. As a result, the calculated weight percentage of PAN in PAN@PVDF-HFP is about 60%.

Electrolyte wettability of the battery separator plays a key role in the overall battery performance. The current commercial battery separator based on PE or PP shows limited electrolyte wettability which affects negatively on the battery performance. Moreover, many surface modifications/coatings made to the commercial separator might also reduce the electrolyte uptake and wettability. Therefore there is a strong demand to tackle this wettability issue. In order to examine the electrolyte wettability of our electrospun fiber network, several tests including the electrolyte uptake measurement, wetting velocity measurement, and contact angle test were conducted on PAN@PVDF-HFP fiber network in comparison to commercial Celgard2400 separator and electrospun PVDF-HFP fiber network (Figure 2b-2d). According to the calculated electrolyte uptake results (Figure 2b), Celgard2400 separator can only absorb about 120 wt% of electrolyte compared to its own weight. In contrast, both the PAN@PVDF-HFP fiber network and electrospun PVDF-HFP fiber network show superior electrolyte wettability of up to 420 wt% electrolyte uptake. In addition to the amount of electrolyte absorbed, the wetting speed is another important factor to examine. Different separators are subjected to the measurements of spreading area of electrolyte with respect to the period of time and the results are compared. As shown in Figure 2c, after

 doi:10.20944/preprints201907.0321.v1

Peer-reviewed version available at *Energies* **2019**, *12*, 3391; doi:10.3390/en12173391



dropping a fixed amount of electrolyte droplet onto the commercial Celgard2400 separator, the electrolyte droplet shows slow spreading even after 50 seconds. For PVDF-HFP and PAN@PVDF-HFP fiber networks, the electrolyte spreads fast with similar speed. The wetting area (round shape) on the separator by the liquid electrolyte droplet increases from 1.00 cm in diameter right after the electrolyte droplet in contact with separator to 1.26 cm in diameter after 10 seconds and 2.14 cm after 50 seconds, respectively. This implies that the PVDF-HFP accounts for the superior wettability to liquid electrolyte and this improvement in electrolyte wettability is huge compared to that for commercial separators. Since lithium ion conduction/transportation during battery operations is always retarded or blocked by the poor wetting property and insufficient electrolyte uptake of separators, it is thus expected that when used as separators, the PVDF-HFP fiber network or the core-shell fiber with PVDF-HFP as the outer layer in contact with electrolyte could have little negative effects on battery performance compared with commercial separators. In addition, the electrolyte contact angle measurements further supports the above conclusion that PVDF-HFP outer layer has superior electrolyte wettability. As shown from Figure 2d, the contact angle of electrolyte droplet on commercial Celgard2400 separator is 54 ° while the contact angle of electrolyte droplet on PAN@PVDF-HFP fiber network is 21 °. Both the contact angles were measured and recorded right after electrolyte droplet in contact with the fiber network.

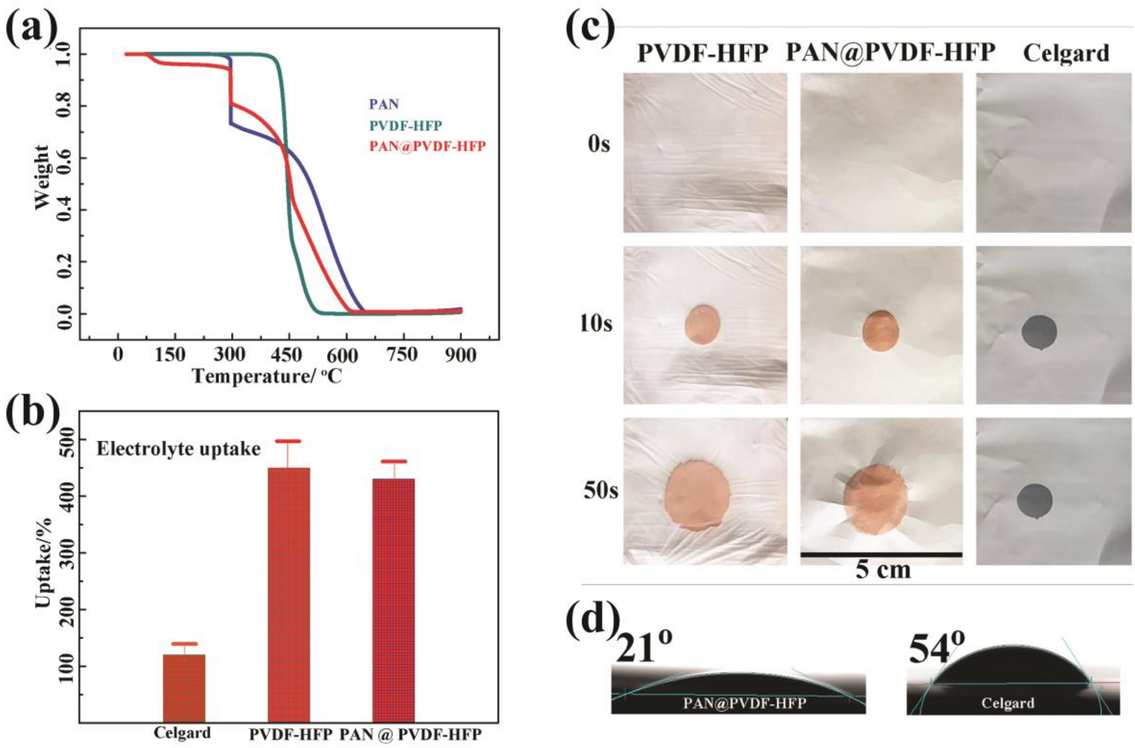


**Figure 2.** (a) TGA curves of PAN, PVDF-HFP and PAN@PVDF-HFP in air flow; (b) The amount of electrolyte uptake for commercial Celgard2400 separator, PVDF-HFP fiber network and PAN@PVDF-HFP fiber network (percentage on the basis of their own weight); (c) The spreading of electrolyte droplet on commercial Celgard2400 separator, PVDF-HFP and PAN@PVDF-HFP fiber network with respect to time; (d) Contact angles of commercial Celgard2400 separator and PAN@PVDF-HFP fiber network in the first second after electrolyte dropping.

Thermal stability is another significant factor for battery separators to investigate. It is well accepted that separator shrinkage under elevated temperature is one of the major origins to the battery thermal runaway [27]. To examine the thermal stability of separators under similar conditions to real battery operations, commercial Celgard2400, PVDF-HFP and PAN@PVDF-HFP fiber network were clamped with two pieces of glass plates first, and were then heated from room temperature to elevated temperature up to 250 °C for 10 min. A piece of brown-colored copper foil

Peer-reviewed version available at Energies 2019, 12, 3391; doi:10.3390/en12173391



was placed at the bottom of glass plates to make the observation clearer and more obvious (Figure S4). As presented in Figure 3, commercial Celgard2400 separator suffers from several shrinkage at 180 °C and non-uniform distribution of pin-holes formation, which could lead to drastically increased short-circuit hotspots and trigger the thermal runaway. At 250 °C the Celgard2400 separator shrinks dramatically and almost disappears. The residual materials turn into dark brown to black color. The PVDF-HFP fiber network also could not endure the high temperature and melts into a transparent viscous layer sticking onto the glass plates (Figure 3) above 180 °C. More typical images demonstrating the melting behavior of PVDF-HFP can be found in Figure S5. In contrast, the PAN@PVDF-HFP fiber network exhibits little shrinking nor does the fiber network melt at elevated temperature up to 250 °C. As a result, the PAN core of the PAN@PVDF-HFP fiber network provides sufficient heat resistance to enable the overall core-shell fiber with excellent thermal stability.


**Figure 3.** The thermal stability tests of commercial Celgard2400 separator, PVDF-HFP and PAN@PVDF-HFP fiber network.

Furthermore, in order to obtain more details about the above temperature-dependent change of separators during heating process, the morphology of these separators were carefully studied using microscopes. Both PVDF-HFP and PAN@PVDF-HFP fiber networks were heated to 180 °C, 200 °C and 250 °C and held at the elevated temperature for 10 min, and then characterized by SEM/EDS. Figure 4 displays the morphology of the two types of separators under different temperatures for 10 min, starting from room temperature. For PAN@PVDF-HFP fiber network, though the PVDF-HFP outer layer gradually melts and shrinks with the increasing temperature, the PAN core serving as skeleton still supports and maintains the entire structure (Figure S6). In comparison, the PVDF-HFP fiber network melts into a viscous fluid which is in accordance with the observations from Figure 3. In addition, the elemental mapping results shown in Figure S7 before and after thermal treatment

Preprints (www.preprints.org) | NOT PEER-REVIEWED | Posted: 28 July 2019 doi:10.20944/preprints201907.0321.v1
Peer-reviewed version available at Energies 2019, 12, 3391; doi:10.3390/en12173391



indicate a uniform distribution of elements carbon (C), nitrogen (N), and fluorine (F) over the entire PAN@PVDF-HFP fiber network.

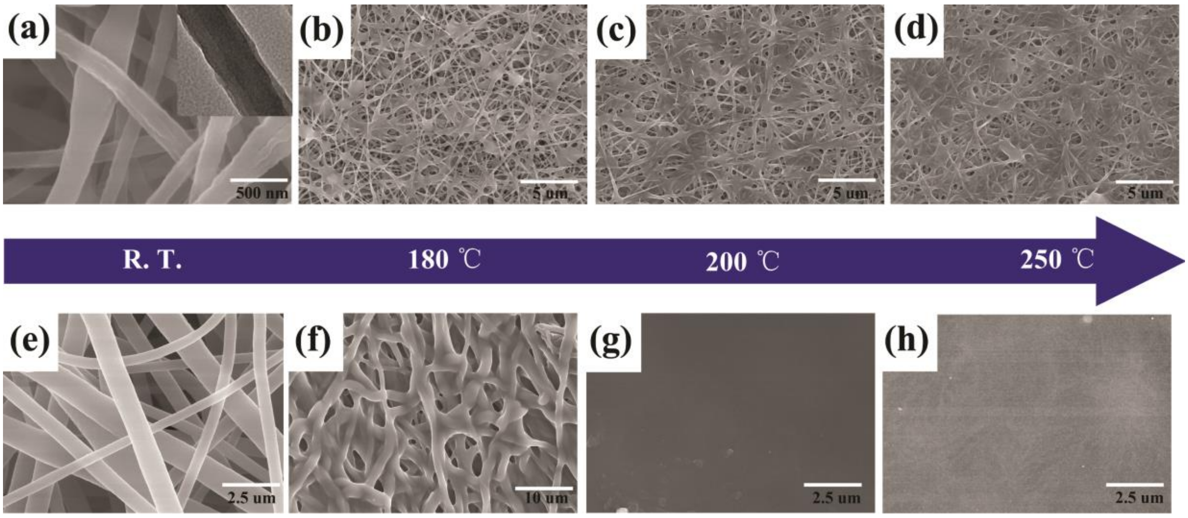


**Figure 4.** The top-view SEM images of the pristine PAN@PVDF-HFP fiber network at (a) room temperature and after thermal treated at (b) 180 °C, (c) 200 °C and (d) 250 °C, respectively; The inset in (a) is the TEM image of a single PAN@PVDF-HFP fiber; The morphology of PVDF-HFP fiber network at (e) room temperature, (f) 180 °C, (g) 200 °C and (h) 250 °C, respectively.

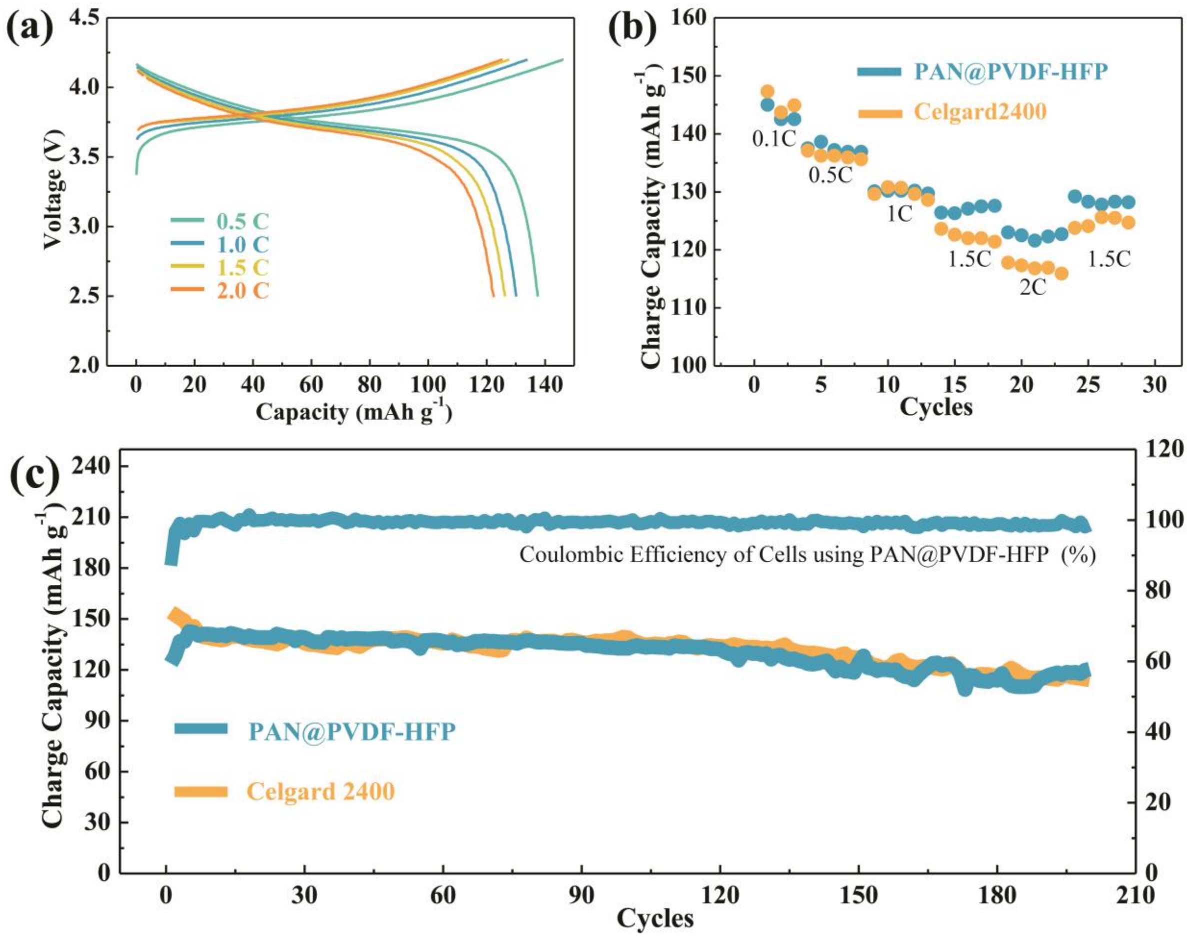


**Figure 5.** The electrochemical performances of NCM cells using Celgard2400 and PAN@PVDF-HFP separators. The voltage range of the cycling is 2.5-4.2 V; (a) The charge-discharge voltage profiles at different C-rates for cells using PAN@PVDF-HFP separators; (b) The rate capability at different C-rates for NCM cells using

Peer-reviewed version available at Energies 2019, 12, 3391; doi:10.3390/en12173391



Celgard2400 and PAN@PVDF-HFP separators; (c) The long-term cycling performances of NCM cells using Celgard2400 and PAN@PVDF-HFP separators.

Finally, lithium-ion batteries using NCM cathodes, Li foil anodes, and the PAN@PVDF-HFP fiber network as separators were constructed and subjected to electrochemical cycling. The voltage profiles at various current rates ranging from 0.5 C to 2 C were demonstrated in Figure 5a, where the cell using NCM cathode and PAN@PVDF-HFP as separator could deliver a high discharge capacity of over 120 mAh $g^{-1}$ even at 2 C rate. Moreover, the rate capability as well as long-term cycling tests were also performed on batteries with NCM cathode and PAN@PVDF-HFP separator. And the results were compared with batteries using same cathode but with commercial Celgard2400 separator. Specifically, as presented in Figure 5b, batteries with PAN@PVDF-HFP separator and PVDF-HFP separator show similar rate behavior under low current rates from 0.1 C to 1 C. However, under the high current rates such as 1.5 C and 2 C, batteries with PVDF-HFP separator exhibit rapid capacity decay and unstable cycling behavior. In contrast, batteries with PAN@PVDF-HFP separator show a superior rate capability with little capacity decay, and the average charge capacity maintains at 128 mAh $g^{-1}$ under 1.5 C and 123 mAh $g^{-1}$ under 2 C, respectively. This improvement in rate capability of batteries with PAN@PVDF-HFP separator compared with commercial separator can be ascribed to the enhanced electrolyte wettability and electrolyte uptake, which triggers facile ion transportation. Furthermore, long-term cycling was conducted on both batteries. And both cells present a good cycling behavior for reversible capacity over 130 mAh $g^{-1}$ for more than 200 cycles with almost 90% capacity retention (Figure 5c). Therefore, the batteries with our dual-nozzle coaxial electrospun core-shell nanofiber as separator show even enhanced electrochemical properties compared with their commercial counterparts.

## 4. Conclusions

In conclusion, the rational design of a core-shell nanofiber network is successfully achieved via our dual-nozzle, coaxial electrospinning technique. This PAN@PVDF-HFP core-shell fiber network with PAN as the core and PVDF-HFP as the outer layer exhibit excellent heat resistance from PAN core and excellent electrolyte wettability from PVDF-HFP shell in the same time. As a result, when used as battery separators, this core-shell fiber network provides superior thermal stability with little compromise or even some enhancement in battery performances. Therefore this core-shell nanofiber as well as this design concept holds promise in next-generation energy storage devices.

**Supplementary Materials:** The following are available online. **Figure S1.** The SEM image of PAN@PVDF-HFP core-shell fiber network. **Figure S2.** The TEM image of two PAN@PVDF-HFP fibers. **Figure S3.** The flexibility test of PAN@PVDF-HFP separator. **Figure S4.** The thermal stability test of commercial separator, PVDF-HFP and PAN@PVDF-HFP fiber network. **Figure S5.** Thermal stability tests of PAN film and PVDF-HFP film at 180 °C. **Figure S6.** SEM image showing the structural intactness of PAN@PVDF-HFP fiber network at 250 °C. **Figure. S7** Elemental mapping of selected area of PAN@PVDF-HFP fiber network.

**Author Contributions:** conceptualization, Y.Z. and Z.L.; methodology, Y.Z.; investigation, Y.L.; writing—original draft preparation, Y.Z.; writing—review and editing, Y.L., Z.L.; supervision, Z.L.; project administration, Y.Z.

**Funding:** The work was supported by the National Natural Science Foundation of China (No. U1564205), Ministry of Science and Technology of China (No. 2013CB934000, 2016YFE0102200).

**Conflicts of Interest:** The authors declare no conflict of interest.

**References**


[1] Miao, Y.; Hynan, P.; von Jouanne, A.; Yokochi, A. Current Li-Ion Battery Technologies in Electric Vehicles and Opportunities for Advancements. *Energies* **2019**, *12*, 1074.

[2] J. B. Goodenough, Y. Kim, Challenges for rechargeable Li batteries, *Chem. Mater.* **2010**, *22*, 587.

[3] J. M. Tarascon, M. Armand, Issues and challenges facing rechargeable lithium batteries, *Nature* **2001**, *414*, 359.

[4] Chen, J. Recent Progress in Advanced Materials for Lithium Ion Batteries. *Materials* **2013**, *6*, 156-183.

[5] Z. Liang, D. C. Lin, J. Zhao, Z. D. Lu, Y. Y. Liu, C. Liu, Y. Y. Lu, H. T. Wang, K. Yan, X. Y. Tao, Y. Cui, Composite lithium metal anode by melt infusion of lithium into a 3D conducting scaffold with lithiophilic coating, *PNAS* **2016**, *113*, 2862.

[6] Y. Zhao, Y. H. Jin, L. Wang, G. Y. Tian, X. M. He, The application of self-assembled hierarchical structures in lithium-ion batteries, *Progress in Chemistry*, **2018**, *30*, 1761-1769.

[7] Z. Liang, K. Yan, G. Zhou, A. Pei, J. Zhao, Y. Sun, J. Xie, Y. Li, F. Shi, Y. Liu, D. Lin, K. Liu, H. Wang, H. Wang, Y. Lu, Y. Cui, Composite lithium electrode with mesoscale skeleton via simple mechanical deformation, *Sci. Adv.* **2019**, *5*, eaau5655.

[8] Y. Zhao, Y. Q. Kang, Y. H. Jin, L. Wang, G. Y. Tian, X. M. He, Recent Progress of Silicon-Based and -Related Materials for Lithium-Ion Batteries, *Progress in Chemistry*, **2019**, *31*, DOI: 10.7536/PC180916.

[9] Z. Liang, X. Tao, Y. Cui, Black TiO2 Nanomaterials for Lithium–Sulfur Batteries, *Black TiO2 Nanomaterials for Energy Applications*, **2017**, 275-304, DOI: 10.1142/9781786341662_0011.

[10] W. X. Ji, F. Wang, D. T. Liu, J. F. Qian, Y. L. Cao, Z. X. Chen, H. X. Yang, X. P. Ai, Building thermally stable Li-ion batteries using a temperature-responsive cathode, *J. Mater. Chem. A* **2016**, *4*, 11239.

[11] K. Liu, Y. Y. Liu, D. C. Lin, A. Pei, Y. Cui, Materials for lithium-ion battery safety, *Sci. Adv.* **2018**, *4*, eaas9820.

[12] K. T. Lee, S. Jeong, J. Cho, Roles of surface chemistry on safety and electrochemistry in lithium ion batteries, *Acc. Chem. Res.* **2013**, *46*, 1161.

[13] H. Li, D. B. Wu, J. Wu, L. Y. Dong, Y. J. Zhu, X. L. Hu, Flexible, high-wettability and fire-resistant separators based on hydroxyapatite nanowires for advanced lithium-ion batteries, *Adv. Mater.* **2017**, *29*, 1703548.

[14] X. N. Feng, M. G. Ouyang, X. Liu, L. G. Lu, Y. Xia, X. M. He, Thermal runaway mechanism of lithium ion battery for electric vehicles: A review, *Energy Storage Materials* **2018**, *10*, 246.

[15] H. Lee, M. Yanilmaz, O. Toprakci, K. Fu, X. W. Zhang, A review of recent developments in membrane separators for rechargeable lithium-ion batteries, *Energy Environ. Sci.* **2014**, *7*, 3857.

[16] H. Zhang, M. Y. Zhou, C. E. Lin, B. K. Zhu, Progress in polymeric separators for lithium ion batteries, *RSC Adv.* **2015**, *5*, 89848.

[17] X. M. Zhu, X. Y. Jiang, X. P. Ai, H. X. Yang, Y. L. Cao, A highly thermostable ceramic-grafted microporous polyethylene separator for safer lithium-ion batteries, *ACS Appl. Mater. Interfaces* **2015**, *7*, 24119.

[18] X. Z. Yan, Y. R. Wang, T. Yu, H. Chen, Z. B. Zhao, S. Y. Guan, Polyimide binder by combining with polyimide separator for enhancing the electrochemical performance of lithium ion batteries, *Electrochimica Acta* **2016**, *216*, 1.

[19] L. Pan, H. B. Wang, C. L. M. Wu, C. B. Liao, L. Li, Tannic-acid-coated polypropylene membrane as a separator for lithium-ion batteries, *ACS Appl. Mater. Interfaces* **2015**, *7*, 16003.

[20] D. Z. Wu, L. Deng, Y. Sun, K. S. Teh, C. Shi, Q. L. Tan, J. B. Zhao, D. H. Sun, L. W. Lin, A high-safety PVDF/$Al_2O_3$ composite separator for Li-ion batteries via tip-induced electrospinning and dip-coating, *RSC Adv.* **2017**, *7*, 24410.

[21] N. Q. Liang, J. H. Fang, X. X. Guo, A simple approach for preparation of porous polybenzimidazole membranes as a promising separator for lithium ion batteries, *J. Mater. Chem. A* **2017**, *5*, 15087.

[22] P. Pankaj Arora, Z. M. Zhang, Battery separators, *Chem. Rev.* **2004**, *104*, 4419.

 doi:10.20944/preprints201907.0321.v1

Peer-reviewed version available at *Energies* **2019**, *12*, 3391; doi:10.3390/en12173391



[23] J. K. Pi, G. P. Wu, H. C. Yang, C. G. Arges, Z. K. Xu, Separators with biomineralized zirconia coatings for enhanced thermo- and electro-performance of lithium-ion batteries, *ACS Appl. Mater. Interfaces* **2017**, *9*, 21971.

[24] X. M. Zhu, X. Y. Jiang, X. P. Ai, H. X. Yang, Y. L. Cao, A highly thermostable ceramic-grafted microporous polyethylene separator for safer lithium-ion batteries, *ACS Appl. Mater. Interfaces* **2015**, *7*, 24119.

[25] Sun, G.; Sun, L.; Xie, H.; Liu, J. Electrospinning of Nanofibers for Energy Applications. *Nanomaterials* **2016**, 6, 129.

[26] J. J. Zhang, Z. H. Liu, Q. S. Kong, C. J. Zhang, S. P. Pang, L. P. Yue, X. J. Wang, J. H. Yao, G. L. Cui, Renewable and superior thermal-resistant cellulose-based composite nonwoven as lithium-ion battery separator, *ACS Appl. Mater. Interfaces* **2013**, *5*, 128.

[27] J. H. Dai, C. Shi, C. Li, X. Shen, L. Q. Peng, D. Z. Wu, D. H. Sun, P. Zhang, J. B. Zhao, A rational design of separator with substantially enhanced thermal features for lithium-ion batteries by the polydopamine-ceramic composite modification of polyolefin membranes, *Energy Environ. Sci.* **2016**, *9*, 3252.

[28] S. Gong, H. Jeon, H. Lee, M. H. Ryou, Y. M. Lee, Effects of an integrated separator/electrode assembly on enhanced thermal stability and rate capability of lithium-ion batteries, *ACS Appl. Mater. Interfaces* **2017**, *9*, 17814.

[29] F. Croce, M. L. Focarete, J. Hassoun, I. Meschini, B. Scrosati, A safe, high-rate and high-energy polymer lithium-ion battery based on gelled membranes prepared by electrospinning, *Energy Environ. Sci.* **2011**, *4*, 921.

[30] X. M. Zhu, X. Y. Jiang, X. P. Ai, H. X. Yang, Y. L. Cao, $TiO_2$ ceramic-grafted polyethylene separators for enhanced thermostability and electrochemical performance of lithium-ion batteries, *J. Membr. Sci.* **2016**, *504*, 97.

[31] S. M. Kang, M. H. Ryou, J. C. Choi, H. Lee, Mussel- and diatom-inspired silica coating on separators yields improved power and safety in Li-ion batteries, *Chem. Mater.* **2012**, *24*, 3481.

[32] M. H. Liu, P. P. Zhang, L. T. Gou, Z. Y. Hou, B. Huang, Enhancement on the thermostability and wettability of lithium-ion batteries separator via surface chemical modification, *Materials Letters* **2017**, *208*, 98.

[33] T. H. Cho, M. Tanaka, H. Onishi, Y. Kondo, T. Nakamura, H. Yamazaki, S. Tanase, T. Sakai, Battery performances and thermal stability of polyacrylonitrile nano-fiber-based nonwoven separators for Li-ion battery, *J. Power Sources* **2008**, *181*, 155.

[34] L. Cao, P. An, Z. Xu, J. Huang, Performance evaluation of electrospun polyimide non-woven separators for high power lithium-ion batteries, *J. Electroanal. Chem.* **2016**, *767*, 34.

[35] D. Bansal, B. Meyer, M. Salomon, Gelled membranes for Li and Li-ion batteries prepared by electrospinning, *J. Power Sources* **2008**, *178*, 848.

[36] Z. Li, W. Q. Wang, Y. Han, L. Zhang, S. S. Li, B. Tang, S. M. Xu, Z. H. Xu, Ether modified poly(ether ether ketone) nonwoven membrane with excellent wettability and stability as a lithium ion battery separator, *J. Power Sources* **2018**, *378*, 176.

[37] C. M. Costa, M. Maria, M. M. Silva, S. Lanceros-Méndez, Battery separators based on vinylidene fluoride (VDF) polymers and copolymers for lithium ion battery applications, *RSC Adv.* **2013**, *3*, 11404.

[38] K. Xiao, Y. Y. Zhai, J. Y. Yu, B. Ding, Nanonet-structured poly(m-phenylene isophthalamide)-polyurethane membranes with enhanced thermostability and wettability for high power lithium ion batteries, *RSC Adv.* **2015**, *5*, 55478.